ARTHRITIS & RHEUMATISM
Vol. 60, No. 6, June 2009, pp 1764–1774
DOI 10.1002/art.24523

Time Course and Nature of Brain Atrophy in the MRL Mouse Model of Central Nervous System Lupus

John G. Sled,[1] Shoshana Spring,[2] Matthijs van Eede,[2] Jason P. Lerch,[1] Sangeeta Ullal,[3] and Boris Sakic[4]

Objective. **Similar to patients with systemic lupus erythematosus, autoimmune MRL/lpr mice spontaneously develop behavioral deficits and pathologic changes in the brain. Given that the disease-associated brain atrophy in this model is not well understood, the present study was undertaken to determine the time course of morphometric changes in major brain structures of autoimmune MRL/lpr mice.**

Methods. **Computerized planimetry and high-resolution magnetic resonance imaging (MRI) were used to compare the areas and volumes of brain structures in cohorts of mice that differ in severity of lupus-like disease.**

Results. **A thinner cerebral cortex and smaller cerebellum were observed in the MRL/lpr substrain, even before severe autoimmunity developed. With progression of the disease, the brain area of coronal sections became smaller and the growth of the hippocampus was retarded, which likely contributed to the increase in the ventricle area:brain area ratio. MRI revealed reduced volume across different brain regions, with the structures in the vicinity of the ventricular system particularly affected. The superior colliculus, periaqueductal gray matter, pons, and midbrain were among the regions most affected, whereas the volumes of the parietal-temporal lobe, parts of the cerebellum, and lateral ventricles in autoimmune MRL/lpr mice were comparable with values in congenic controls.**

Conclusion. **These results suggest that morphologic alterations in the brains of MRL/lpr mice are a consequence of several factors, including spontaneous development of lupus-like disease. A periventricular pattern of parenchymal damage is consistent with the cerebrospinal fluid neurotoxicity, limbic system pathologic features, and deficits in emotional reactivity previously documented in this model.**

Neuropsychiatric (NP) manifestations are a common and serious complication of systemic lupus erythematosus (SLE). Contemporary imaging techniques have revealed various abnormalities in patients with SLE, including lesions in the periventricular and subcortical regions (1,2), hypoperfusion (3), and regional metabolic abnormalities (4). Brain atrophy is the most frequent observation (5) and is likely a consequence of widespread neuronal and glial damage (6). Consistent with these reports, recent studies on water diffusivity indicate a genuine loss of brain-tissue integrity in patients with NPSLE/central nervous system (CNS) lupus (7). However, the lack of understanding of CNS damage led to development of animal models of acute and chronic lupus and dissection of complex pathogenic circuits (8).

MRL/MpJTnfrsf6^{lpr} (MRL/lpr) mice and MRL/MpJ+/+ (MRL+/+) congenic control mice share more than 99.9% of their genome but differ in the onset of lupus-like manifestations. The 3–4-month difference in the time to onset allows discrimination of autoimmunity-induced functional and structural brain damage from epiphenomena associated with aging and with damage of vital peripheral organs (9). In addition to accelerated development of serologic signs of inflammation and autoimmunity, MRL/lpr mice develop, at an early stage, a constellation of behavioral deficits and neuropathologic changes, operationally termed autoimmune-

Supported by the Canadian Institutes for Health Research and the Ontario Research and Development Challenge Fund.

[1]John G. Sled, PhD, Jason P. Lerch, PhD: Hospital for Sick Children, and University of Toronto, Toronto, Ontario, Canada; [2]Shoshana Spring, MSc, Matthijs van Eede, MCSc: Hospital for Sick Children, Toronto, Ontario, Canada; [3]Sangeeta Ullal, BSc: McMaster University, Hamilton, Ontario, Canada; [4]Boris Sakic, PhD: McMaster University, and St. Joseph's Healthcare, Hamilton, Ontario, Canada.

Address correspondence and reprint requests to Boris Sakic, PhD, McMaster University, Department of Psychiatry and Behavioral Neurosciences, The Brain-Body Institute, St. Joseph's Healthcare, Juravinski Innovation Center T-3307, 50 Charlton Avenue East, Hamilton, Ontario L8N 4A6, Canada. E-mail: sakic@mcmaster.ca.

Submitted for publication December 2, 2008; accepted in revised form February 17, 2009.

associated behavioral syndrome (AABS). In models of CNS lupus, AABS has been shown to have significant face, construct, and predictive validity (10). In particular, reduced complexity of pyramidal neurons, retarded brain growth (11,12), increased TUNEL staining (13), Fluoro Jade B positivity (14), and increased ubiquitination in the cerebral cortex and limbic system (15) are all manifestations that point to profound neurodegeneration in the brain parenchyma of these mice. The common occurrence of enlarged ventricles in diseased MRL/lpr mice further supports the causal link between systemic autoimmunity and loss of brain tissue (16,17).

CNS lupus has focal, diffuse, and complex forms of presentation. The focal form is characterized by cerebral infarctions and peripheral neuropathies, while the diffuse form is often associated with brain atrophy, psychiatric manifestations, and cognitive decline; the complex form involves manifestations of both disease types. To understand the nature of brain atrophy in the MRL mouse model, it is important to elucidate its time course and whether the loss of brain parenchyma is either generalized or selected. Previous evidence from behavioral and neuropathologic studies points to the periventricular region and the nearby limbic structures as primary targets of intrathecal autoimmune activity (15,18–21). Although neuronal damage was also noted in the cortical and cerebellar areas, it was neither quantified nor compared with damage in other brain regions (14).

The aim of the present study was to assess regional changes in the brains of MRL substrains of mice during the progression of lupus-like disease. In the first experiment, digital planimetry was used to measure the areas of major brain structural changes in cohorts of differing age and varying disease severity. In the second experiment, high-resolution magnetic resonance imaging (MRI) was used to examine volumetric differences in specific brain regions and nuclei. The overall expectation was that changes in the limbic system will be detected at the onset of autoimmune disease, when anxiety-related and depression-like behavioral deficits emerge in MRL/lpr mice (18,20).

MATERIALS AND METHODS

Assessment of the time course of planimetric changes in major brain structures (experiment 1). *Animals and tissue collection.* Infiltrated immunocytes can be seen in the choroid plexus of some MRL/lpr mice as young as age 8 weeks (22). Given that the median life span of this substrain is ~20 weeks, these time points were used to assign cohorts into 3 general age groups for the assessment of the time course of gross morphologic changes. In particular, 5–8-week-old mice were assigned to the young age group, 9–20-week-old mice were assigned to the middle age group, and mice older than age 20 weeks were assigned to the old age group.

Eighty-one MRL/lpr mice and 47 MRL+/+ mice, ranging in age from 5 weeks to 48 weeks, were originally purchased at 4 weeks of age from The Jackson Laboratory (Bar Harbor, ME) to measure organ weights. Of this group, 39 MRL/lpr mice and 26 MRL+/+ mice of both sexes were also used for planimetric analysis. Mice were housed in groups of 4 per cage and were kept under standard laboratory conditions (light period from 7:00 AM to 7:00 PM, room temperature ~21°C, humidity ~62%, regular rodent chow and tap water ad libitum, bedding changed every 3–4 days). Many of the MRL/lpr mice older than age 3 months developed overt symptoms, as evidenced by lymph node enlargement, necrotic ear tips, dermatitis, and alopecia.

Mice were anesthetized with an intraperitoneal injection of pentobarbital sodium (Somnotol; 65 mg/kg, 0.15–0.2 ml) and their body weight was recorded. After intracardial perfusion with 40 ml phosphate buffered saline (PBS), the brains were removed within 2 minutes and weighed on a digital scale (Mettler Toledo AB54-S; VWR Scientific of Canada, Mississauga, Ontario, Canada). The brains were then immersed into 4% paraformaldehyde and transferred 48 hours later into bottles with 30% sucrose–PBS. Given that splenomegaly is a hallmark of lupus-like disease in the MRL/lpr substrain, the wet spleen weight was measured upon extraction. All experimental protocols were approved by a local animal care committee and carried out in accordance with the rules and regulations of the Canadian Council of Animal Care.

Planimetric analysis. Sealed bottles were sent by courier to NeuroScience Associates Laboratory (Knoxville, TN) for sectioning and staining of the mouse brains. Twenty mouse brains were leveled, embedded in a gelatin block, and simultaneously cut coronally. The sections were processed using a standard hematoxylin and eosin staining protocol. Slides were examined under a laser scanning microscope (LSM 510; Zeiss, Wetzlar, Germany). Digital images were obtained with a 10×/0.63 objective and Nikon digital camera at a resolution of 1,024 × 1,024 pixels, and subsequently traced with Axiovision software, version 4.5 (Zeiss). The areas of interest included the entire brain area, the thickness of the motor, sensory, and piriform cortices, and the areas of the lateral ventricles, hippocampus, and cerebellum. A standard atlas of the mouse brain was used for locating specific cerebral and cerebellar regions.

The brain area was assessed on 16 sections at the following approximate locations (in mm from Bregma): 2.34, 2.22, 1.18, 0.98, 0.02, −0.22, −0.70, −1.22, −1.70, −1.94, −2.18, −2.70, −3.40, −3.52, −4.16, and −4.32. These sections were selected because they were undamaged on all brains examined. For the first 2 sections, the shapes of the medial orbital cortex and the intrabulbar commissure (anterior part) were used as landmarks. In the subsequent 7 sections, the size and shape of the lateral ventricles were used for slice comparisons. In the posterior 7 sections, the size and shape of the hippocampus were used to match sections from different brains.

The thickness of the secondary (M2) and primary (M1) motor cortices, the sensory cortex, and the piriform cortex was measured bilaterally on 6 sections, at the following approximate locations (in mm from Bregma): 1.18, 0.98, 0.02, −0.22,

−0.70, and −1.22. The cortical surface was the starting point, while the ending points were the cingulum, dorsal end of the external capsule, laterodorsal striatum, and ventral endopiriform nucleus, respectively. The left and right lateral ventricles were traced on 3 sections, at 1.18, −0.70, and −1.22 mm from Bregma. The left and right hippocampi were measured on 6 planes, at −1.70, −1.94, −2.18, −3.40, −3.64, and −4.16 mm from Bregma. The hippocampi were flanked by the corpus callosum on the dorsal side, lateral ventricle and fimbria on the lateral side, and the third ventricle on the medial side. The cerebellum was measured on 5 sections, at −5.80, −6.00, −6.12, −6.24, and −6.48 mm from Bregma. The tracing included the fourth and fifth cerebellar lobules, tenth cerebellar lobule, inferior cerebellar peduncle, simple lobule, Crus-1 and -2 of ansiform lobules, and paraflocculus. The fourth ventricle was used as a landmark for the ventral boundary of the cerebellum.

Statistical analysis. The data were analyzed by two-way analysis of variance (ANOVA). The between-group factors were substrain (MRL/lpr versus MRL+/+) and age (young, middle, and old), while values obtained from different sections or hemispheres in the same mouse were treated as repeated measures. Student's *t*-test was used in the post hoc group comparison. Pearson's and Spearman's correlation procedures were used to measure associations between dependent variables. All computations were performed with SPSS software (version 13; SPSS, Chicago, IL) and FigP software (version 2.98; Biosoft, Cambridge, UK). Results of brain planimetry are expressed as the mean ± SEM. *P* values less than 0.05 were considered significant.

Assessment of volumetric differences by MRI (experiment 2). *Animals and sample preparation.* Based on the significant group differences that were revealed by brain planimetry, separate cohorts of adult MRL/lpr and MRL+/+ mice were used to study volumetric differences in 3-dimensionally defined brain regions. High-resolution MRI was used to determine the volumes of 62 regions, which were identified with reference to a standard atlas of the mouse brain.

This experiment was conducted on a cohort of 12-week-old MRL/lpr (n = 14) and MRL+/+ (n = 17) male mice, born in colonies at McMaster University and The Jackson Laboratory. Mice were housed under the same conditions as described in experiment 1. Body and spleen weights were recorded at the time that the mice were killed. The mice were anesthetized with a combination of ketamine (100 mg/kg; Pfizer, Kirkland, Quebec, Canada) and rompun (20 mg/kg; Bayer, Toronto, Ontario, Canada) via intraperitoneal injection. The thoracic cavities were exposed, and 30 ml of PBS, pH 7.4, kept at room temperature, was infused at a rate of ~100 ml/hour through the left ventricle. This was followed by infusion with 30 ml of iced 4% paraformaldehyde in PBS at the same rate. Following perfusion, the heads were removed along with the skin, lower jaw, ears, and cartilaginous nose tip. The remaining skull structures were allowed to postfix in 4% paraformaldehyde at 4°C for 12 hours. Following an incubation period of 5 days in PBS and 0.01% sodium azide at 15°C, the skulls were transferred to a contrast agent solution of PBS and 2 m*M* gadoteridol (ProHance; Bracco Diagnostics, Princeton, NJ) for at least 7 days at 15°C. MRI was performed at least 21 days postmortem.

Imaging and processing. A multichannel 7.0-Tesla MRI scanner (Varian, Palo Alto, CA) with a 6-cm–inner bore diameter insert-gradient set was used to acquire anatomic images of the brains within the skulls. Prior to imaging, the samples were removed from the contrast agent solution, blotted, and placed into 13-mm–diameter plastic tubes filled with a proton-free susceptibility-matching fluid (Fluorinert FC-77; 3M Corporation, St. Paul, MN). Three custom-built, 14-mm–diameter solenoid coils with a length of 18.3 mm and overwound ends were used to image 3 brains in parallel. The parameters used in the scans were optimized for grey/white matter contrast, as follows: T2-weighted, 3-dimensional fast spin-echo sequence, repetition time/echo time 325/32 msec, echo train length 6, 4 averages, field of view 14 × 14 × 25 mm, and matrix size 432 × 432 × 780 mm, giving an image with 32 μm isotropic voxels. The total imaging time was 11.3 hours.

The obtained 32-μm isotropic resolution T2-weighted MRI scans were then nonlinearly aligned to a 3-dimensional atlas of the mouse brain with 62 structures identified. As described in more detail previously (23), this process consisted of a 3-part registration scheme involving an initial rigid body alignment, followed by a set of 12-parameter pairwise registrations between all mice, and finally, a set of iterative nonlinear registrations. An additional processing step was required to adapt the above-summarized algorithm to the MRL mouse strain. Forty percent of specimens showed a fluid layer surrounding the brain that was bright on T2-weighted MR images and that prevented accurate identification of the cortical surface by the algorithm. This was addressed in these specimens by attenuating the intensity of this layer to match that of the surrounding meninges and skull. This step consisted of normalizing the median image intensity of all scans, manually training an intensity-based classifier in which fluid and parenchyma had Gaussian-distributed intensity models, and computing the normalized likelihood (L) map of fluid for each specimen. Within a region ~100 μm inside and outside of the initial estimate of the cortical surface, voxels with a high likelihood of being fluid were substituted with the intensity of the skull (I_s), and voxels with intermediate likelihoods were assigned values between the intensity of the skull and that of the parenchyma (I_p). The exact substitution formula, based on a normalized likelihood of $L \in [0, 1]$ and selected crispness parameter (γ) of 13, was

$$I = \begin{cases} I & L \le 0.1 \\ (1-\alpha)I_s + \alpha I_p & L > 0.1 \end{cases}$$

where the parameter α was calculated as

$$\alpha = \frac{e^{-\gamma(L-1/2)}}{1+e^{-\gamma(L-1/2)}}.$$

The cortical surface determined without and with this correction is illustrated in Figure 5. The volume of the identified fluid layer was retained for subsequent analysis.

Statistical analysis. The volume for each anatomic structure defined in the atlas was computed for each mouse by integrating the Jacobian of the transformation mapping the atlas image to the image for that mouse. This procedure has previously been shown to provide volume estimates comparable with those obtained by standard stereologic methods using tissue sections (24). The effect of MRL substrain (genotype) on the volume of each structure was assessed by regression

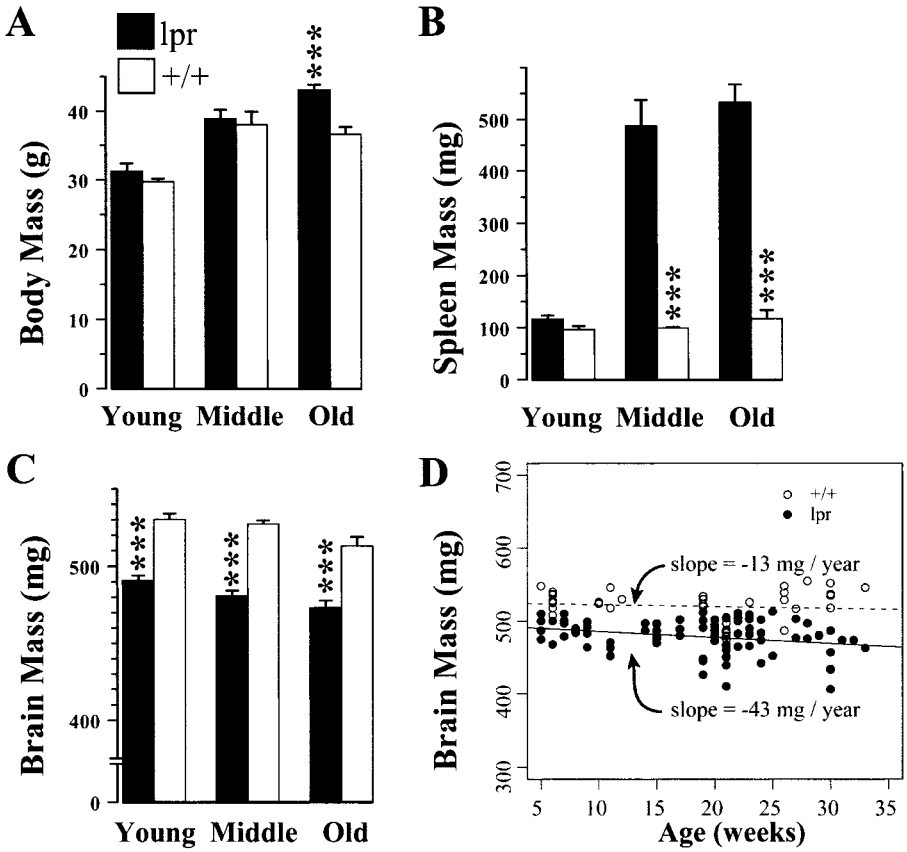

Figure 1. Comparison of body mass and spleen mass between MRL/lpr mice and MRL+/+ control mice by age group. **A,** Body mass was comparable between young and middle-age MRL/lpr mice and their age-matched controls, but the cohort of old MRL/lpr mice was significantly heavier than their controls. **B,** Profound splenomegaly, as indicated by significantly increased spleen mass in the middle-age and old MRL/lpr mice compared with their controls, provided confirmation of the severe autoimmune disease in these groups. **C,** Brain mass was lower in the lupus-prone MRL/lpr mice in all 3 age groups compared with their controls. **D,** Regression slopes of brain weight were plotted against actual age (in weeks). The negative slope for the MRL/lpr group suggests a genuine loss of brain parenchyma with aging and disease progression. Bars in **A–C** show the mean and SEM. *** = $P < 0.05$ versus age-matched MRL+/+ control mice.

against a linear model with genotype as a fixed factor and body weight as a covariate, using the software package R (http://www.r-project.org/). The significance (chance of Type I error) of the *t*-statistic associated with the genotype factor was corrected for multiple comparisons using the false discovery rate method (25). In addition, the relationship between brain volume and the volume of the outside fluid layer was assessed by ANOVA with genotype as a factor and 3 covariates, the fluid volume, the body weight, and the fluid volume–genotype interaction.

Local differences in brain shape related to genotype were assessed by analysis of the deformation fields (26). For this analysis, the transformation data were smoothed with a 0.5-mm Gaussian kernel, and the logarithm of the Jacobian was computed for univariate statistical comparison at every image point. The resulting *t*-statistic images were examined for regions exceeding a significance threshold corresponding to a 5% false discovery rate (for a 2-tailed test).

RESULTS

Changes to major brain structures, as revealed by planimetry in experiment 1. Although body mass was comparable between the MRL/lpr and control mice in the young and middle-age groups, old MRL/lpr mice were significantly heavier than their age-matched controls (substrain-by-age, $F[2,122] = 3.427$, $P = 0.036$; $t[58] = 5.152$, $P < 0.001$) (Figure 1A). As expected, a steep increase in spleen weight in the mice in the middle-age and old groups confirmed the accelerated onset of lupus-like disease in the MRL/lpr substrain (substrain-by-age, $F[2,122] = 10.104$, $P < 0.001$ versus controls) (Figure 1B). Conversely, lighter brains were observed in all MRL/lpr mice compared with the MRL+/+ controls, even those in the young age group (substrain, F[1,122] =

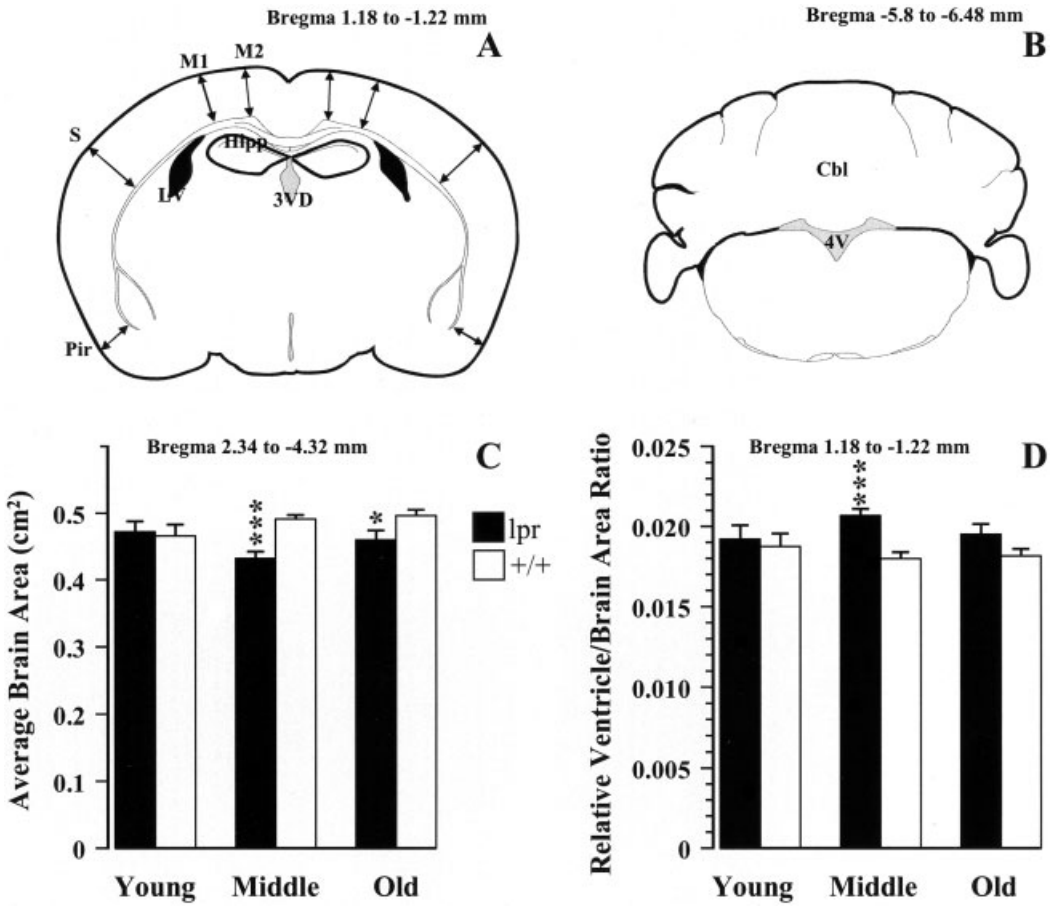

Figure 2. Planimetry and thickness assessments of the brain areas of MRL/lpr mice compared with MRL+/+ congenic controls. **A** and **B,** Schematic representations of the cortical areas (at −1.22 mm from Bregma) **(A)** and the cerebellum (Cbl) (at −6.24 mm from Bregma) **(B)** selected for planimetry and thickness assessments. The section range values are shown above the illustrations. The hippocampal (Hipp) region outlined in **A** is for illustrative purposes only; the actual hippocampal sections measured were at −1.70 mm to −4.16 mm from Bregma. **C** and **D,** Comparison of the brain areas **(C)** and ventricle area:brain area ratios **(D)** in each substrain according to age. Results show that a reduced brain area is concomitant with the onset of lupus-like disease in MRL/lpr mice, and a significantly increased brain area ratio is evident in middle-age MRL/lpr mice. The section range values used to assess the brain areas and area ratios are shown above the graphs. Bars in **C** and **D** show the mean and SEM. $* = P < < 0.05$; $*** = P < 0.001$, versus age-matched MRL+/+ controls. Pir = piriform (cortex); S = sensory (cortex); M1 = primary motor (cortex); LV = lateral ventricle; 3VD = third ventricle dorsal; 4V = fourth ventricle.

91.798, $P < 0.001$; age, F[2,122] = 6.065, $P = 0.003$) (Figure 1C). The comparison of regression slopes (determined using the R software package [27]) revealed a significant between-group difference in brain mass changes over time ($t[124] = -2.74$, $P < 0.01$), with the slope for the MRL/lpr mice declining at an annualized rate of −43 mg/year, compared with no significant decline in brain mass over time in the controls (Figure 1D). No significant correlation was observed between body mass and brain mass when mice of all groups and all ages were considered (r[126] = −0.052, *P* not significant [NS]).

The tracing of major brain regions (shown schematically in Figures 2A and B) revealed numerous differences between the MRL substrains at different ages. Overall, ANOVA revealed a smaller brain area in the MRL/lpr substrain compared with the MRL+/+ controls (substrain, F[1,55] = 6.803, $P = 0.012$), but this analysis was not sensitive in detecting any significant substrain-by-age interaction (F[2,55] = 2.329, $P = 0.1$), likely because of the reduced sample size. However, the *t*-test applied to each age group revealed that the mean brain cross-sectional area was comparable in the young age groups of both substrains, but was smaller in MRL/lpr mice at ages associated with inflammation of the brain (middle age, $t[23] = -3.763$, $P < 0.001$ versus age-matched controls; old age, $t[23] = -2.084$, $P = 0.048$ versus age-matched controls) (Figure 2C).

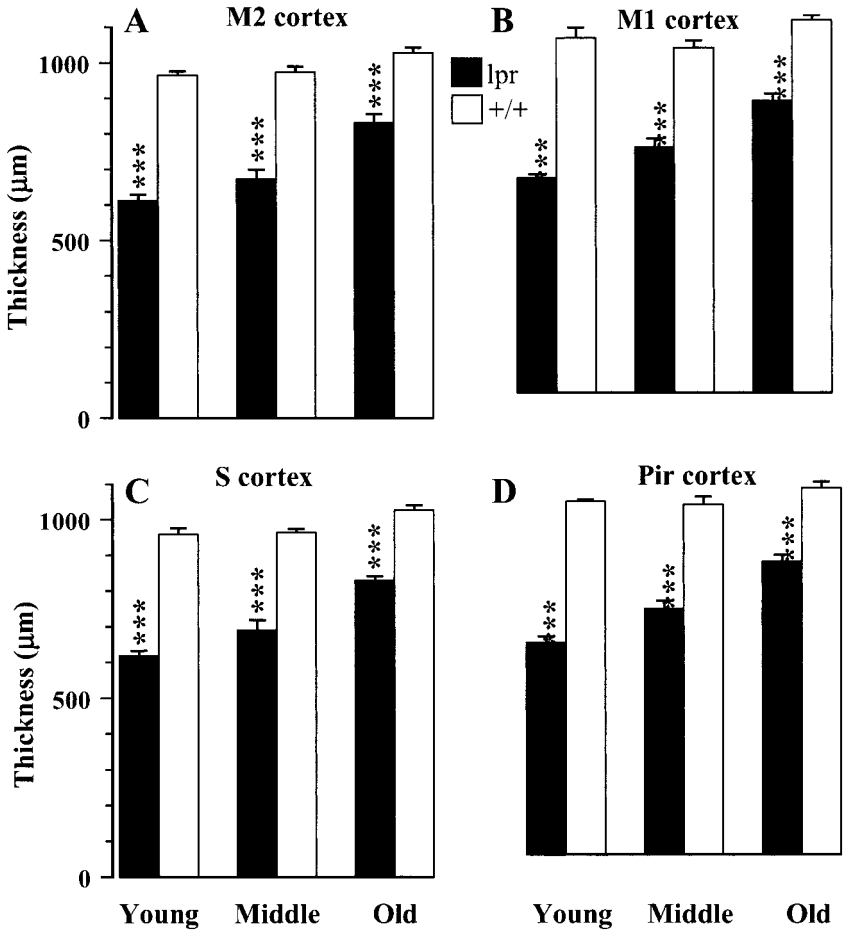

Figure 3. Assessment of cortical thickness in all age groups of MRL/lpr mice and MRL+/+ control mice in the functional brain regions of the secondary (M2) and primary (M1) motor cortices (**A** and **B**) as well as the sensory (S) cortex (**C**) and piriform (Pir) cortex (**D**). Bars show the mean and SEM. *** = $P < 0.05$ versus age-matched MRL+/+ control mice.

The comparisons of ventricle size among the 3 age groups of MRL/lpr mice and control mice revealed no significant between-group differences. However, due to a reduction in mean brain area at the onset of CNS involvement, the relative ventricle area:brain area ratio was significantly increased in the middle-age group of MRL/lpr mice (t[23] = 3.966, $P < 0.001$ versus age-matched controls) (Figure 2D).

All age groups of MRL/lpr mice had a thinner cortex at the secondary and primary levels of the motor cortex (M2 and M1, respectively) and also had thinner sensory and piriform cortices compared with controls (Figures 3A–D). This deficiency was profound in MRL/lpr mice at young age, but attenuated in adulthood (substrain-by-age, at M2, F[2,55] = 4.266, $P = 0.019$; at M1, F[2,55] = 4.539, $P = 0.015$; at the sensory cortex, F[2,55] = 3.906, $P = 0.026$; at the piriform cortex,

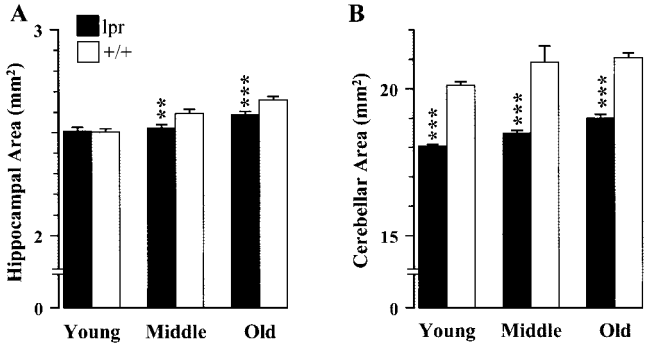

Figure 4. Area of the hippocampus (**A**) and cerebellum (**B**) in all age groups of MRL/lpr mice and MRL+/+ control mice. Hippocampal size was comparable in young MRL/lpr mice, but showed retarded growth in older MRL/lpr mice, concomitant with the onset of severe lupus-like disease (**A**). Cerebellar area was significantly reduced in all age groups of MRL/lpr mice compared with controls (**B**). Bars show the mean and SEM. ** = $P < 0.01$; *** = $P < 0.05$, versus age-matched MRL+/+ control mice.

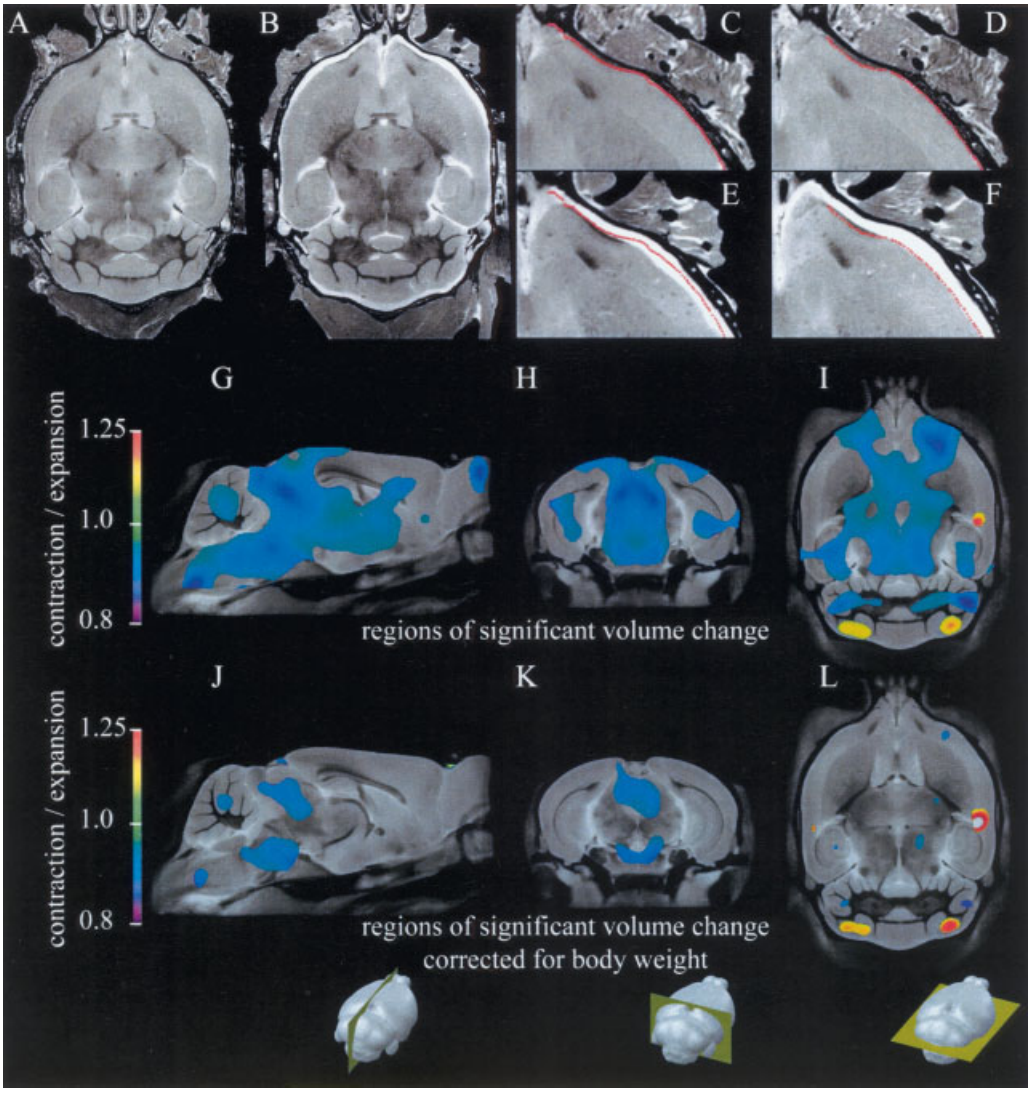

Figure 5. Representative specimens (shown in horizontal section) used for volumetric assessments by magnetic resonance imaging (MRI), illustrating the need to account for fluid appearing between the brain and skull. The image in **A** shows negligible fluid, while in **B,** significant fluid buildup is evident. In **C** and **D** (expanded views of the sample in **A**), the cortical surface was estimated without **(C)** and with **(D)** suppression of the fluid signal. In each case, the estimated cortical surface is shown in red. **E** and **F** are the corresponding expanded views of the sample in **B.** Note the improved estimate of the cortical surface in **F**. Voxel-wise differences between the brains of MRL+/+ and MRL/lpr mice are shown in **G–L.** Local expansion/contraction factors are shown overlaid on an average of the 31 nonlinearly aligned MRI scans. The local volume difference is indicated by the scale on the left, with 1.0 corresponding to no difference. Regions significantly smaller in the MRL/lpr group than in the control group are in blue or purple, and regions significantly larger in the MRL/lpr group are in yellow or red. In **G–I,** regions shown in color were significantly different from controls, as determined by Student's *t*-test, with $t > 2.6$ (degrees of freedom [df] 29), corresponding to a false discovery rate of 5%. **G,** Sagittal section to the left of midline. **H,** Coronal section intersecting the superior and inferior colliculus. **I,** Transverse section at the level indicated by the 3-dimensional icon in yellow. Images in **G–I** show widespread reductions in the brain volume of MRL/lpr mice. In **J–L,** corresponding slices show the effect of genotype on brain volume, after correcting for body weight. The threshold for significance ($t > 3.5$, df 28) corresponds to a false discovery rate of 5%. Note the decreases in the volume of the superior and inferior colliculus, periaqueductal gray matter, and midbrain.

F[2,55] = 4.452, $P = 0.016$). Conversely, the size of the hippocampus in the MRL substrains was comparable between each substrain in the young age group (t[9] = 0.209, P NS), but its growth was retarded in the middle-age and old MRL/lpr groups compared with their age-matched MRL+/+ controls (substrain, F[1,55] = 7.164, $P < 0.01$) (Figure 4A).

Finally, MRL/lpr mice of all ages had smaller cerebellums than did their congenic controls, but the size of the cerebellum increased with age at the same

rate as seen in the control group (substrain, F[1,55] = 128.179, $P < 0.001$; age, F[2,55] = 7.292, $P = 0.002$) (Figure 4B). Taken together, the obtained results suggest that the brain of the MRL/lpr mouse is lighter, the cortex is thinner, and the cerebellum is smaller than that of the MRL+/+ substrain. In addition, an increased ventricle area:brain area ratio and shrinking hippocampus are associated with the development of lupus-like disease.

Brain volumetric data, as revealed by MRI in experiment 2. The cohort of MRL/lpr mice obtained from The Jackson Laboratory was lighter than their MRL+/+ controls (mean ± SD body weight 43.0 ± 3.5 gm versus 46.6 ± 3.5 gm; $P = 0.008$). Both genotypes showed a fluid layer around the brain in ~40% of specimens (Figures 5A–F). Consistent with the reduced brain area observed in experiment 1 in MRL/lpr mice, the overall brain volume in MRL/lpr mice was smaller than in MRL+/+ controls (mean ± SD 0.48 ± 0.03 ml versus 0.52 ± 0.02 ml; $P < 0.008$). When these data were corrected for the difference in body weight, this corresponded to an effect of substrain (genotype) on brain volume of 0.02 ml. When a false discovery rate of 5% was assumed, 46 of the 62 structures were found to be significantly smaller in MRL/lpr mice than in MRL+/+ congenic control mice, after correcting for body weight. A complete list of the volumes of each brain structure, corresponding to anatomic regions defined in the atlas, is given in Table 1.

A statistical parametric map of local volume differences revealed a few regions that deviated from the overall linear trend of smaller brain size in MRL/lpr mice. The volumes of the superior colliculus, periaqueductal gray matter, pons, and midbrain in MRL/lpr mice were profoundly reduced relative to the overall brain volume, whereas a bilateral portion of the parietal-temporal lobe and parts of the cerebellum were less decreased in volume. This localized pattern was seen either in analyses without correction for the difference in body weight (Figures 5G–I) or when this factor was considered a covariate (Figures 5J–L). In summary, the MRI analysis revealed a high degree of bilateral symmetry, a widespread volume reduction in a majority of regions, and profound effects in areas bordering the ventricular system in diseased MRL/lpr mice.

DISCUSSION

The present study reveals significant morphologic changes in the brains of autoimmune MRL/lpr mice. Reductions in brain parenchyma are evident even at young age, as characterized by a lower brain mass, reduced thickness of cortical regions, and smaller cerebellum. Moreover, further declines in the overall brain area and hippocampal size suggest that early pathologic changes in CNS lupus show progression in adult MRL/lpr mice. The MRI analysis revealed significantly reduced volumes in a majority of brain regions and nuclei, most notably in the vicinity of the ventricular system. These findings support the hypothesis that the early onset of lupus-like disease retards brain growth and leads to a neurodegenerative phenotype (11,14). Moreover, these results are consistent with evidence that the emergence of systemic autoimmunity and inflammation renders cerebrospinal fluid neurotoxic to periventricular areas of the limbic system, thus producing lesions that underlie deficits in emotional reactivity and motivated behavior (15,18,28).

Several mechanisms may account for the observed pathologic changes in the brain before the SLE-like disease fully manifests. First, MRL/lpr mice have a dysfunctional Fas receptor in immune and other somatic cells. The lack of normal apoptotic signaling in the brain (29) may lead to aberrant embryogenesis and postnatal development (30). Second, an early up-regulation in systemic interleukin-6 (31) may compromise the immature blood–brain barrier and induce detrimental changes in neurogenesis (32). Last, given that autoimmune dams are used (at ~3–4 months of age) in the production of MRL/lpr pups, one may assume that full-blown maternal disease affects normal development of the embryonic brain. Indeed, CNS involvement in neonatal lupus has been documented by computed tomography; a majority of infant mice whose mothers were affected by SLE had brain abnormalities, including reduced attenuation of the cerebral white matter, reduced subcortical white matter, basal ganglia calcifications, and enlarged ventricles (33). Along the same line, experimental studies revealed that mouse offspring develop profound deficiencies in behavior when wild-type embryos are reared in an autoimmune uterine environment (34). More recently, reduced cortical thickness and anti-NMDA receptor binding in the ventricular zone have been observed in mouse offspring exposed in utero to neurotoxic autoantibodies from dams with lupus-like disease (35). A teratogenic role of maternal autoantibodies is also proposed from studies showing the toxicity of human SLE immunoglobulins on rat embryos (36) and significant correlation to learning disability in children of mothers with SLE (37).

In addition to an overall reduction in brain volume in most brain regions, the limbic and midbrain structures are particularly reduced in MRL/lpr mice. The observation of disease-related hippocampal atrophy

Table 1. Volume of atlas-identified brain structures in autoimmune MRL/lpr mice compared with MRL+/+ congenic controls

Anatomic region	Volume, mean ± SD μl		% difference in volume	P^*
	MRL+/+	MRL/lpr		
Colliculus superior	9.28 ± 0.36	8.29 ± 0.46	−12.0	0.0005
Pontine nucleus	2.01 ± 0.07	1.83 ± 0.08	−9.4	0.0007
Periaqueductal gray	9.42 ± 0.37	8.55 ± 0.42	−10.1	0.0012
Pons	29.62 ± 1.08	27.18 ± 1.21	−9.0	0.0016
Cerebral aqueduct	1.56 ± 0.05	1.44 ± 0.06	−8.4	0.0026
Fourth ventricle	1.07 ± 0.03	0.99 ± 0.05	−8.0	0.0026
Interpedunclar nucleus	1.26 ± 0.04	1.17 ± 0.05	−7.7	0.0026
Inferior cerebellar peduncle	0.99 ± 0.03	0.91 ± 0.05	−8.4	0.0046
Medulla	55.27 ± 2.51	50.49 ± 2.57	−9.5	0.0046
Midbrain	22.63 ± 0.97	20.56 ± 1.25	−10.0	0.0046
Dentate gyrus of hippocampus	4.35 ± 0.17	4.02 ± 0.21	−8.1	0.0057
Stria medullaris	1.14 ± 0.04	1.06 ± 0.05	−7.8	0.0057
Cuneate nucleus	1.18 ± 0.04	1.10 ± 0.05	−7.3	0.0059
Mammillary bodies	1.30 ± 0.04	1.21 ± 0.06	−7.6	0.0059
Posterior commissure	1.14 ± 0.05	1.05 ± 0.05	−8.1	0.0059
Superior cerebellar peduncle	1.00 ± 0.04	0.92 ± 0.05	−8.5	0.0068
Colliculus inferior	5.25 ± 0.22	4.82 ± 0.28	−9.0	0.0068
Facial nerve; cranial nerve 7	1.07 ± 0.04	1.00 ± 0.05	−7.5	0.0068
Lateral olfactory tract	1.73 ± 0.07	1.60 ± 0.08	−8.0	0.0068
Thalamus	16.70 ± 0.78	15.30 ± 0.87	−9.1	0.0085
Middle cerebellar peduncle	1.75 ± 0.06	1.64 ± 0.07	−6.4	0.0097
Habenular commissure	0.80 ± 0.03	0.75 ± 0.04	−7.5	0.0097
Hippocampus	19.58 ± 0.86	18.12 ± 0.93	−8.1	0.0097
Mammilothalamic tract	0.72 ± 0.03	0.67 ± 0.03	−7.7	0.0097
Bed nucleus of stria terminalis	1.92 ± 0.08	1.77 ± 0.10	−8.4	0.0105
Olfactory bulbs	18.88 ± 0.75	17.64 ± 0.75	−7.0	0.0105
Medial lemniscus medial longitudinal fasciculus	2.55 ± 0.14	2.33 ± 0.13	−9.5	0.0112
Anterior commissure pars anterior	1.63 ± 0.08	1.50 ± 0.09	−9.2	0.0114
Arbor vita of cerebellum	7.93 ± 0.31	7.39 ± 0.37	−7.4	0.0132
Stria terminalis	1.39 ± 0.06	1.29 ± 0.07	−8.1	0.0142
Third ventricle	2.03 ± 0.08	1.89 ± 0.10	−7.2	0.0159
Anterior commissure pars posterior	1.58 ± 0.06	1.47 ± 0.08	−7.4	0.0165
Fasciculus retroflexus	1.62 ± 0.06	1.51 ± 0.08	−7.2	0.0165
Fornix	1.38 ± 0.06	1.28 ± 0.07	−7.7	0.0171
Fimbria	3.65 ± 0.16	3.38 ± 0.19	−7.9	0.0171
Superior olivary complex	1.28 ± 0.06	1.18 ± 0.07	−8.4	0.0178
Internal capsule	3.03 ± 0.14	2.81 ± 0.17	−8.1	0.0179
Subependymale zone rhinocele	0.59 ± 0.02	0.55 ± 0.03	−7.3	0.0179
Stratum granulosum of hippocampus	2.38 ± 0.11	2.21 ± 0.13	−8.1	0.0190
Ventral tegmental decussation	1.02 ± 0.04	0.95 ± 0.05	−7.6	0.0197
Corticospinal tract pyramids	2.29 ± 0.15	2.09 ± 0.12	−9.7	0.0219
Inferior olivary complex	0.90 ± 0.04	0.83 ± 0.05	−8.5	0.0219
Globus pallidus	3.57 ± 0.15	3.32 ± 0.18	−7.4	0.0230
Cerebral peduncle	2.89 ± 0.12	2.69 ± 0.16	−7.5	0.0240
Lateral septum	3.44 ± 0.17	3.19 ± 0.18	−7.8	0.0297
Corpus callosum	15.60 ± 0.84	14.33 ± 1.01	−8.9	0.0450
Occipital lobe	5.75 ± 0.20	5.35 ± 0.37	−7.4	0.0510
Optic tract	1.29 ± 0.06	1.20 ± 0.07	−7.5	0.0510
Fundus of striatum	1.34 ± 0.06	1.25 ± 0.07	−7.0	0.0778
Striatum	22.60 ± 1.38	20.80 ± 1.40	−8.7	0.0912
Cerebellar cortex	48.10 ± 1.64	45.49 ± 2.60	−5.8	0.0971
Nucleus accumbens	4.59 ± 0.26	4.25 ± 0.29	−7.9	0.1194
Medial septum	2.55 ± 0.13	2.38 ± 0.15	−7.3	0.1336
Basal forebrain	6.69 ± 0.35	6.22 ± 0.43	−7.5	0.1497
Frontal lobe	41.72 ± 2.32	38.85 ± 2.57	−7.4	0.1897
Hypothalamus	8.69 ± 0.50	8.11 ± 0.55	−7.2	0.2293
Olfactory tubercle	3.73 ± 0.23	3.50 ± 0.24	−6.6	0.3489
Pre para subiculum	2.42 ± 0.13	2.26 ± 0.17	−7.2	0.3514
Lateral ventricle	3.03 ± 0.16	2.86 ± 0.17	−5.7	0.4056
Parieto-temporal lobe	69.04 ± 3.93	65.41 ± 4.11	−5.6	0.6501
Amygdala	14.61 ± 0.97	13.93 ± 1.04	−4.8	0.6775
Entorhinal cortex	8.73 ± 0.39	8.36 ± 0.46	−4.5	0.7275

* P values were determined by t-test, after corrections for body weight and multiple comparisons.

is not surprising, since this is consistent with the neurodegenerative changes observed in SLE patients and in MRL/lpr mice at the onset of autoimmune disease (14,15). Immune-mediated mechanisms, such as antibody-mediated neurotoxicity (28,38), are likely critical for the terminal damage of brain tissue. Moreover, an early disturbance in the activity of the hypothalamus–pituitary–adrenal axis and elevated levels of serum corticosterone at baseline (39) may play a permissive or facilitatory role by increasing neuronal vulnerability; namely, this endocrine imbalance leads to sustained binding of corticosterone to its receptors in the hippocampus and induces hippocampal dysfunction and reductions in hippocampal volume, as shown in other models of chronic disease (40). Along the same line, a smaller midbrain and hippocampus are consistent with the notion of an anxious/depression-like behavioral profile (18,20,41), deficits in spatial learning/memory tasks (42), proclivity to self-injurious behavior, and altered dopamine receptor expression in substantia nigra of diseased MRL/lpr mice (43).

The present results add to the face validity of the MRL model by revealing an aspect that is consistent with the findings from CNS lupus imaging. In particular, it is documented that magnetization transfer ratios, an MRI metric sensitive to the detection of demyelination and atrophy, are abnormal in patients with CNS lupus (44), as is water diffusivity assessed by diffusion-weighted MRI (7). The absence of focal injury in the MRL/lpr model is consistent with MRI findings in humans indicating that SLE patients with neuropsychiatric symptoms show diffuse brain injury (45) with evidence of demyelination, axonal loss, and atrophy (46). A recent clinical study that used quantitative diffusion imaging and diffusion anisotropy showed decreased anisotropy in the genu corpus callosum and anterior internal capsule of SLE patients (47). Although other changes may be unique to the anatomy of the human brain, these observations match the findings of reduced volumes of corpus callosum and internal capsule in diseased MRL/lpr mice.

As further evidence of neurodegeneration, N-acetyl aspartate, a marker of neuronal viability measured by magnetic resonance spectroscopy (MRS), is also reduced in CNS lupus (48) and is expressed at lower levels in patients whose brains show significant atrophy (49). Similarly, an experimental study that used MRS revealed increased water content in MRL/lpr brains, indicative of edema (50). In addition, the levels of glutamine, glutamate, and lactate were higher in the brains of MRL/lpr mice than in controls.

In summary, the present study reveals profound neuroanatomic changes in the lupus-prone MRL/lpr substrain that are likely mediated by several mechanisms. An age-dependent decline in brain mass and hippocampal size are consistent with a cascade of pathogenic events. They include cerebrospinal fluid–mediated cytotoxicity, impaired neurogenesis, and neurodegeneration in the limbic system that accounts for early changes in emotional reactivity. By providing evidence of disease-associated damage of the hippocampus and a periventricular pattern of brain damage, the validity of the MRL model is further strengthened as a way of understanding brain damage in patients with SLE.

ACKNOWLEDGMENTS

We are thankful to Mrs. Julie Switzer (NeuroScience Associates Laboratory) for timely processing of brain tissue samples, and to Dr. Bob Switzer for providing constructive comments.

AUTHOR CONTRIBUTIONS

All authors were involved in drafting the article or revising it critically for important intellectual content, and all authors approved the final version to be published. Dr. Sakic had full access to all of the data in the study and takes responsibility for the integrity of the data and the accuracy of the data analysis.

Study conception and design. Sled, Lerch, Sakic.
Acquisition of data. Sled, Spring, Lerch, Ullal, Sakic.
Analysis and interpretation of data. Sled, van Eede, Lerch, Sakic.

REFERENCES

1. Brooks WM, Sabet A, Sibbitt WL, Barker PB, van Zijl PC, Duyn JH, et al. Neurochemistry of brain lesions determined by spectroscopic imaging in systemic lupus erythematosus. J Rheumatol 1997;24:2323–9.
2. Jennings JE, Sundgren PC, Attwood J, McCune J, Maly P. Value of MRI of the brain in patients with systemic lupus erythematosus and neurologic disturbance. Neuroradiology 2004;46:15–21.
3. Lopez-Longo FJ, Carol N, Almoguera MI, Olazaran J, Alonso-Farto JC, Ortega A, et al. Cerebral hypoperfusion detected by SPECT in patients with systemic lupus erythematosus is related to clinical activity and cumulative tissue damage. Lupus 2003;12:813–9.
4. Yoshida A, Shishido F, Kato K, Watanabe H, Seino O. Evaluation of cerebral perfusion in patients with neuropsychiatric systemic lupus erythematosus using 123I-IMP SPECT. Ann Nucl Med 2007;21:151–8.
5. Waterloo K, Omdal R, Jacobsen EA, Klow NE, Husby G, Torbergsen T, et al. Cerebral computed tomography and electroencephalography compared with neuropsychological findings in systemic lupus erythematosus. J Neurol 1999;246:706–11.
6. Trysberg E, Nylen K, Rosengren LE, Tarkowski A. Neuronal and astrocytic damage in systemic lupus erythematosus patients with central nervous system involvement. Arthritis Rheum 2003;48:2881–7.
7. Welsh RC, Rahbar H, Foerster B, Thurnher M, Sundgren PC. Brain diffusivity in patients with neuropsychiatric systemic lupus erythematosus with new acute neurological symptoms. J Magn Reson Imaging 2007;26:541–51.
8. Alexander JJ, Quigg RJ. Systemic lupus erythematosus and the brain: what mice are telling us. Neurochem Int 2007;50:5–11.
9. Sakic B, Szechtman H, Talangbayan H, Denburg SD, Carbotte RM, Denburg JA. Behaviour and immune status of MRL mice in the postweaning period. Brain Behav Immun 1994;8:1–13.

10. Sakic B, Szechtman H, Denburg JA. Neurobehavioral alteration in autoimmune mice. Neurosci Biobehav Rev 1997;21:327–40.
11. Sakic B, Szechtman H, Denburg JA, Gorny G, Kolb B, Whishaw IQ. Progressive atrophy of pyramidal neuron dendrites in autoimmune MRL/lpr mice. J Neuroimmunol 1998;87:162–70.
12. Sakic B, Kolb B, Whishaw IQ, Gorny G, Szechtman H, Denburg JA. Immunosuppression prevents neuronal atrophy in lupus-prone mice: evidence for brain damage induced by autoimmune disease? J Neuroimmunol 2000;111:93–101.
13. Sakic B, Maric I, Koeberle PD, Millward JM, Szechtman H, Maric D, et al. Increased TUNEL-staining in brains of autoimmune Fas-deficient mice. J Neuroimmunol 2000;104:147–54.
14. Ballok DA, Millward JM, Sakic B. Neurodegeneration in autoimmune MRL/lpr mice as revealed by Fluoro Jade B staining. Brain Res 2003;964:200–10.
15. Ballok DA, Woulfe J, Sur M, Cyr M, Sakic B. Hippocampal damage in mouse and human forms of systemic autoimmune disease. Hippocampus 2004;14:649–61.
16. Denenberg VH, Sherman GF, Rosen GD, Morrison L, Behan PO, Galaburda AM. A behavior profile of the MRL/Mp lpr/lpr mouse and its association with hydrocephalus. Brain Behav Immun 1992;6:40–9.
17. Sakic B, Hanna SE, Millward JM. Behavioral heterogeneity in an animal model of neuropsychiatric lupus. Biol Psychiatry 2005;57: 679–87.
18. Sakic B, Szechtman H, Talangbayan H, Denburg SD, Carbotte RM, Denburg JA. Disturbed emotionality in autoimmune MRL-lpr mice. Physiol Behav 1994;56:609–17.
19. Ballok DA, Earls AM, Krasnik C, Hoffman SA, Sakic B. Autoimmune-induced damage of the midbrain dopaminergic system in lupus-prone mice. J Neuroimmunol 2004;152:83–97.
20. Sakic B, Denburg JA, Denburg SD, Szechtman H. Blunted sensitivity to sucrose in autoimmune MRL/lpr mice: a curve-shift study. Brain Res Bull 1996;41:305–11.
21. Maric D, Millward JM, Ballok DA, Szechtman H, Barker JL, Denburg JA, et al. Neurotoxic properties of cerebrospinal fluid from behaviorally impaired autoimmune mice. Brain Res 2001; 920:183–93.
22. Vogelweid CM, Johnson GC, Besch-Williford CL, Basler J, Walker SE. Inflammatory central nervous system disease in lupus-prone MRL/lpr mice: comparative histologic and immunohistochemical findings. J Neuroimmunol 1991;35:89–99.
23. Dorr AE, Lerch JP, Spring S, Kabani N, Henkelman RM. High resolution three-dimensional brain atlas using an average magnetic resonance image of 40 adult C57Bl/6J mice. Neuroimage 2008;42:60–9.
24. Lerch JP, Carroll JB, Dorr A, Spring S, Evans AC, Hayden MR, et al. Cortical thickness measured from MRI in the YAC128 mouse model of Huntington's disease. Neuroimage 2008;41:243–51.
25. Benjamini Y, Hochberg Y. Controlling the false discovery rate: a practical and powerful approach to multiple testing. J R Stat Soc B 1995;57:289–300.
26. Nieman BJ, Flenniken AM, Adamson SL, Henkelman RM, Sled JG. Anatomical phenotyping in the brain and skull of a mutant mouse by magnetic resonance imaging and computed tomography. Physiol Genomics 2006;24:154–62.
27. Zar JH. Biostatistical analysis. 4th ed. New York: Prentice-Hall; 1999.
28. Sakic B, Kirkham DL, Ballok DA, Mwanjewe J, Fearon IM, Macri J, et al. Proliferating brain cells are a target of neurotoxic CSF in systemic autoimmune disease. J Neuroimmunol 2005;169:68–85.
29. Park C, Sakamaki K, Tachibana O, Yamashima T, Yamashita J, Yonehara S. Expression of Fas antigen in the normal mouse brain. Biochem Biophys Res Commun 1998;252:623–8.
30. Ishimura R, Martin GR, Ackerman SL. Loss of apoptosis-inducing factor results in cell-type-specific neurogenesis defects. J Neurosci 2008;28:4938–48.
31. Tang B, Matsuda T, Akira S, Nagata N, Ikehara S, Hirano T, et al. Age-associated increase in interleukin 6 in MRL/lpr mice. Int Immunol 1991;3:273–8.
32. Vallieres L, Campbell IL, Gage FH, Sawchenko PE. Reduced hippocampal neurogenesis in adult transgenic mice with chronic astrocytic production of interleukin-6. J Neurosci 2002;22:486–92.
33. Prendiville JS, Cabral DA, Poskitt KJ, Au S, Sargent MA. Central nervous system involvement in neonatal lupus erythematosus. Pediatr Dermatol 2003;20:60–7.
34. Denenberg VH, Mobraaten LE, Sherman GF, Morrison L, Schrott LM, Waters NS, et al. Effects of the autoimmune uterine/maternal environment upon cortical ectopias, behavior and autoimmunity. Brain Res 1991;563:114–22.
35. Lee JY, Huerta PT, Zhang J, Kowal C, Bertini E, Volpe BT, et al. Neurotoxic autoantibodies mediate congenital cortical impairment of offspring in maternal lupus. Nat Med 2009;15:91–6.
36. Nadler DM, Klein NW, Aramli LA, Chambers BJ, Mayes M, Wener MH. The direct embryotoxicity of immunoglobulin G fractions from patients with systemic lupus erythematosus. Am J Reprod Immunol 1995;34:349–55.
37. Ross G, Sammaritano L, Nass R, Lockshin M. Effects of mothers' autoimmune disease during pregnancy on learning disabilities and hand preference in their children. Arch Pediatr Adolesc Med 2003;157:397–402.
38. DeGiorgio LA, Konstantinov KN, Lee SC, Hardin JA, Volpe BT, Diamond B. A subset of lupus anti-DNA antibodies cross-reacts with the NR2 glutamate receptor in systemic lupus erythematosus. Nat Med 2001;7:1189–93.
39. Lechner O, Dietrich H, Oliveira dos Santos A, Wiegers GJ, Schwarz S, Harbutz M, et al. Altered circadian rhythms of the stress hormone and melatonin response in lupus-prone MRL/MP-fas^{lpr} mice. J Autoimmun 2000;14:325–33.
40. Sapolsky RM. Glucocorticoids and hippocampal atrophy in neuropsychiatric disorders. Arch Gen Psychiatry 2000;57:925–35.
41. Sakic B, Gurunlian L, Denburg SD. Reduced aggressiveness and low testosterone levels in autoimmune MRL/lpr males. Physiol Behav 1998;63:305–9.
42. Sakic B, Szechtman H, Denburg SD, Carbotte RM, Denburg JA. Spatial learning during the course of autoimmune disease in MRL mice. Behav Brain Res 1993;54:57–66.
43. Chun S, McEvilly R, Foster JA, Sakic B. Proclivity to self-injurious behavior in MRL/lpr mice: implications for autoimmunity-induced damage in the dopaminergic system. Mol Psychiatry 2008;13: 1043–53.
44. Bosma GP, Rood MJ, Zwinderman AH, Huizinga TW, van Buchem MA. Evidence of central nervous system damage in patients with neuropsychiatric systemic lupus erythematosus, demonstrated by magnetization transfer imaging. Arthritis Rheum 2000;43:48–54.
45. Huizinga TW, Steens SC, van Buchem MA. Imaging modalities in central nervous system systemic lupus erythematosus. Curr Opin Rheumatol 2001;13:383–8.
46. Csepany T, Bereczki D, Kollar J, Sikula J, Kiss E, Csiba L. MRI findings in central nervous system systemic lupus erythematosus are associated with immunoserological parameters and hypertension. J Neurol 2003;250:1348–54.
47. Zhang L, Harrison M, Heier LA, Zimmerman RD, Ravdin L, Lockshin M, et al. Diffusion changes in patients with systemic lupus erythematosus. Magn Reson Imaging 2007;25:399–405.
48. Chinn RJ, Wilkinson ID, Hall-Craggs MA, Paley MN, Shorthall E, Carter S, et al. Magnetic resonance imaging of the brain and cerebral proton spectroscopy in patients with systemic lupus erythematosus. Arthritis Rheum 1997;40:36–46.
49. Sibbitt WL Jr, Haseler LJ, Griffey RH, Hart BL, Sibbitt RR, Matwiyoff NA. Analysis of cerebral structural changes in systemic lupus erythematosus by proton MR spectroscopy. AJNR Am J Neuroradiol 1994;15:923–8.
50. Alexander JJ, Zwingmann C, Quigg R. MRL/lpr mice have alterations in brain metabolism as shown with [^{1}H-^{13}C] NMR spectroscopy. Neurochem Int 2005;47:143–51.